Intercalation of hydrotalcites with hexacyanoferrate(II) and (III)—a thermoRaman spectroscopic study

Ray L. Frost*, Anthony W. Musumeci, Jocelyn Bouzaid, Moses O. Adebajo, Wayde N. Martens, J. Theo Kloprogge

Inorganic Materials Research Program, School of Physical and Chemical Sciences, Queensland University of Technology, GPO Box 2434, Brisbane Queensland 4001, Australia

Abstract

Raman spectroscopy using a hot stage indicates that the intercalation of hexacyanoferrate(II) and (III) in the interlayer space of a Mg, Al hydrotalcites leads to layered solids where the intercalated species is both hexacyanoferrate(II) and (III). Raman spectroscopy shows that depending on the oxidation state of the initial hexacyanoferrate partial oxidation and reduction takes place upon intercalation. For the hexacyanoferrate(III) some partial reduction occurs during synthesis. The symmetry of the hexacyanoferrate decreases from O_h existing for the free anions to D_{3d} in the hexacyanoferrate interlayered hydrotalcite complexes. Hot stage Raman spectroscopy reveals the oxidation of the hexacyanoferrate(II) to hexacyanoferrate(III) in the hydrotalcite interlayer with the removal of the cyanide anions above 250 °C. Thermal treatment causes the loss of CN ions through the observation of a band at 2080 cm^{-1}. The hexacyanoferrate (III) interlayered Mg, Al hydrotalcites decomposes above 150 °C.
© 2005 Elsevier Inc. All rights reserved.

Keywords: Hydrotalcite; Brucite; Raman microscopy; Hexacyanoferrate(III); Potassium hexacyanoferrate(II)

1. Introduction

Hydrotalcites, or layered double hydroxides (LDHs) are fundamentally anionic clays [1]. The structure of hydrotalcite can be derived from a brucite structure ($Mg(OH)_2$) in which, e.g., Al^{3+} or Fe^{3+} (pyroaurite-sjögrenite) substitutes a part of the Mg^{2+} [2–8]. The nature of the cations in the hydroxide layers and of the interlayer anions can be varied substantially. This substitution of the trivalent cation for the divalent cation creates a positive layer charge on the hydroxide layers, which is compensated by interlayer anions or anionic complexes [9,10]. Some ternary systems may also be synthesized and characterised such as the system based upon Co and Cu as the divalent cation with Fe as the trivalent cation [11]. When LDHs are synthesized any appropriate counter charge balancing anion can be placed in the interlayer. Calcinations of the hydrotalcites leads to the formation of mixed oxides. In the particular case of hydrotalcites containing iron the properties of the final oxides depends on the location of the iron in the brucite-like layers or in the complex anion in the interlayer. Typically the counter anion may be any anion with a suitable negative charge including the hexacyanoferrate(II) and hexacyanoferrate(III) ions [12–20]. The incorporation of these ions has implications in electrochemistry [17,19,21–23]. The hydrotalcite may be considered as a gigantic cation which is counterbalanced by anions in the interlayer. In hydrotalcites a broad range of compositions are possible of the type $[M^{2+}_{1-x}M^{3+}_x(OH)_2][A^{n-}]_{x/n} \cdot yH_2O$, where M^{2+} and M^{3+} are the di- and trivalent cations in the octahedral positions within the hydroxide layers with x normally between 0.17 and 0.33. A^{n-} is an exchangeable interlayer anion [24]. Normally, the carbonate anion is the major

*Corresponding author. Fax: +61 7 3864 1804.
E-mail address: r.frost@qut.edu.au (R.L. Frost).

interlayer counter anion. Of course when synthesizing hydrotalcites any anion may be used [4,25–28]. Reevesite and pyroaurite are based upon the incorporation of carbonate into the interlayer with d(003) spacings of around 8 Å [29,30]. Normally the hydrotalcite structure based upon takovite (Ni,Al) and hydrotalcite (Mg,Al) has basal spacings of ~8.0 Å where the interlayer anion is carbonate. The concentration of particular anion may also effect the d(003) spacing of the hydrotalcite [31].

The potential application of hydrotalcites as catalysts rests with the ability to make mixed metal oxides at the atomic level, rather than at a particle level. Such mixed metal oxides are formed through the thermal decomposition of the hydrotalcite [32,33]. There are many other important uses of hydrotalcites such as in the removal of environmental hazards in acid mine drainage [34,35], and a mechanism for the disposal of radioactive wastes [36]. Their ability to exchange anions presents a system for heavy metal removal from contaminated waters [37]. Structural information on different minerals has successfully been obtained recently by sophisticated thermal analysis techniques [38–43]. In order to gain insight into the redox processes taking place in the interlayer, we report the hot stage Raman spectroscopy of hydrotalcite with hexacyanoferrate(II) and hexacyanoferrate(III) in the interlayer as a function of temperature.

2. Experimental

2.1. Synthesis of hydrotalcite compounds

A mixed solution of aluminium and magnesium nitrates ($[Al^{3+}] = 0.25$ M and $[Mg^{2+}] = 0.75$ M; 1 M = 1 mol/dm^3) and a mixed solution of sodium hydroxide ($[OH^-] = 2$ M) and the desired anion, at the appropriate concentration, were placed in two separate vessels and purged with nitrogen for 20 min (all compounds were dissolved in freshly decarbonated water). The cationic solution was added to the anions via a peristaltic pump at 40 mL/min and the pH maintained above 9 with the addition of 0.1 M NaOH. The mixture was then aged at 75 °C for 18 h under a N$_2$ atmosphere. The resulting precipitate was then filtered thoroughly with room temperature decarbonated water to remove nitrates and left to dry in a vacuum desiccator for several days. The presence of nitrates (and carbonates) is readily checked quite quickly by obtaining the Raman spectrum of the synthesized hydrotalcite. The nitrate and carbonate anions are characterised by intense sharp bands at 1047 and 1070 cm^{-1}, respectively. In this way phase-pure hydrotalcites with different anions in the interlayer were synthesized. The phase composition was checked by X-ray diffraction (XRD) and the chemical composition by EDXA analyses.

2.2. X-ray diffraction

XRD patterns were collected using a Philips X'pert wide angle X-ray diffractometer, operating in step scan mode, with CuKα radiation (1.54052 Å). Patterns were collected in the range 3–90° 2θ with a step size of 0.02° and a rate of 30 s per step. Samples were prepared as a finely pressed powder into aluminium sample holders. The Profile Fitting option of the software uses a model that employs twelve intrinsic parameters to describe the profile, the instrumental aberration and wavelength dependent contributions to the profile.

2.3. Infrared spectroscopy

Infrared spectra were obtained using a Nicolet Nexus 870 FTIR spectrometer with a smart endurance single bounce diamond ATR cell. Spectra over the 4000–525 cm^{-1} range were obtained by the co-addition of 64 scans with a resolution of 4 cm^{-1} and a mirror velocity of 0.6329 cm/s. Spectra were co-added to improve the signal-to-noise ratio.

2.4. Raman spectroscopy

The crystals of hydrotalcite minerals were placed and orientated on a polished metal surface on the stage of an Olympus BHSM microscope, which is equipped with 10× and 50× objectives. The microscope is part of a Renishaw 1000 Raman microscope system, which also includes a monochromator, a filter system and a charge coupled device (CCD). A Spectra-Physics model 127 He–Ne laser (633 nm) at a resolution of 2 cm^{-1} in the range between 100 and 4000 cm^{-1} was used for Raman excitation. Repeated acquisition, using the highest magnification, was accumulated to improve the signal-to-noise ratio in the spectra. Spectra were calibrated using the 520.5 cm^{-1} line of a silicon wafer. Powers of less than 1 mW at the sample were used to avoid laser induced degradation of the sample. Slight defocusing of the laser beam also assists in the preservation of the sample. Spectra at elevated temperatures were obtained in an air atmosphere using a Linkam thermal stage (Scientific Instruments Ltd., Waterfield, Surrey, England).

Spectroscopic manipulation such as baseline adjustment, smoothing and normalisation were performed using the Spectracalc software package GRAMS (Galactic Industries Corporation, NH, USA). Band component analysis was undertaken using the Jandel 'Peakfit' software package, which enabled the type of fitting function to be selected and allows specific parameters to be fixed or varied accordingly. Band fitting was done using a Gauss–Lorentz cross-product function with the minimum number of component bands used for the fitting process. The Gauss–Lorentz

ratio was maintained at values greater than 0.7 and fitting was undertaken until reproducible results were obtained with squared correlations of r^2 greater than 0.995.

3. Results and discussion

3.1. X-ray diffraction

The XRD patterns for the hexacyanoferrate(II) and hexacyanoferrate(III) interlayered hydrotalcites are shown in Fig. 1. For comparison the XRD patterns of the sulphate and carbonate interlayered hydrotalcite are shown. The XRD patterns clearly show the formation of the hydrotalcites with the different anions in the interlayer. The XRD patterns also show no impurities in the synthesized hydrotalcites. Hydrotalcite normally has a $d(003)$ spacing of 7.9 Å. The sulphate interlayered hydrotalcite has a spacing of 8.0 Å. The hexacyanoferrate(II) complex has a spacing of 10.9 Å and the hexacyanoferrate(III) hydrotalcite 11.1 Å. The increased interlayer spacing is due to the size of the anion between the brucite-like layers.
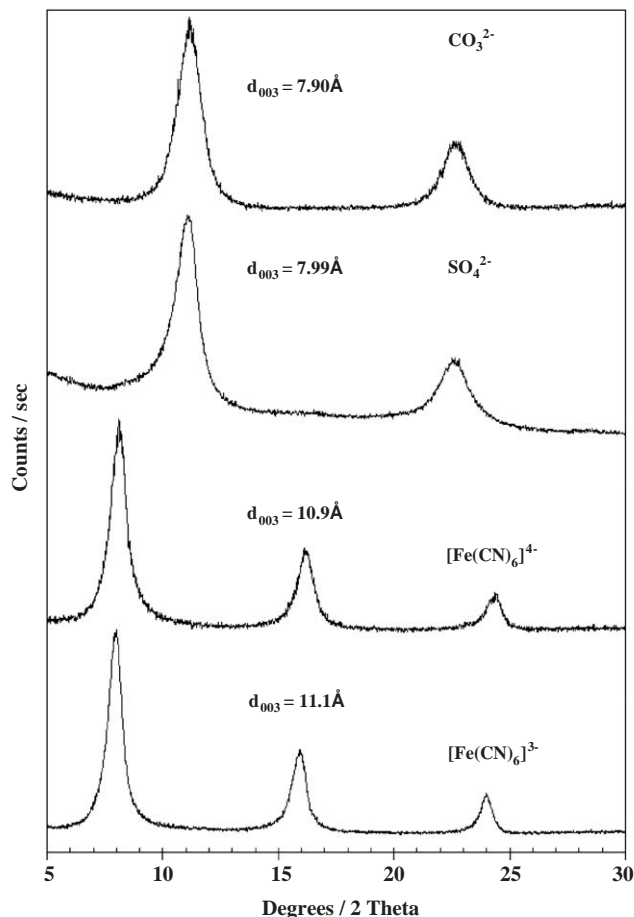

Fig. 1. Powder XRD patterns of the samples used in this study.

3.2. Raman spectroscopy

The structure of the hexacyanoferrate anion is a regular octahedron with six cyanide ligands at each site with a symmetry of O_h. The selection rules show that the vibrational modes A_{1g}, E_g and T_{2g} will be Raman active only. The T_{1u} mode will be infrared active only. The C_3-axis of this octahedron is oriented perpendicular to the hydrotalcite brucite-like hydroxyl sheets [18,44]. Braterman et al. reasoned that the CN vibrations would correspond to the vibrational modes A_{1g}, E_g and T_{1u}. The fact that the first two modes are observed in the infrared spectrum as low intensity bands provides an indication of symmetry reduction. The T_{1u} mode is split into two modes assigned to E_u and A_{2u}. This is indicative of a reduction in symmetry from O_h to D_{3d}.

The Raman spectra of the potassium hexacyanoferrate (II) and (III) ions are shown in Fig. 2a. The hexacyano anion is characterised by bands at 2092 and $2064 \, cm^{-1}$ for the potassium hexacynaoferrate(II) salt and at 2133 and $2126 \, cm^{-1}$ for the potassium hexacynaoferrate(III). Bands in these positions are assigned to the CN stretching vibrations. In addition two sets of low intensity bands are observed in the Raman spectra of the potassium hexacyanoferrate(III) at 2079, 2077 and at 2095 and $2091 \, cm^{-1}$ (Fig. 2b). These bands correspond to the positions for the potassium hexacyanoferrate (II). The presence of bands attributable to the CN stretching vibrational modes of the hexacyanoferrate(II) in the spectra of hexacyanoferrate(III) are also confirmed by the infrared spectra. The infrared spectra of the potassium hexacyanoferrate (II) and (III) are characterised by bands at 2032 (Fe(II)) and 2113 and 2041 (Fe(III)) cm^{-1} (Fig. 3). A previous study also found an additional band for the hexacyanoferrate(III) at $2076 \, cm^{-1}$ [25]. The band position of the free CN^- ion is $2084 \, cm^{-1}$. The band at $2076 \, cm^{-1}$ seems to correspond to the free CN^- ion. The two bands at 2091 and $2076 \, cm^{-1}$ correspond with the band positions for the potassium hexacyanoferrate (II) salt. This simply shows that there is some Fe(II) impurity in the Fe(III) compound.

A change in oxidation state of the iron in the hexacyanoferrate complexes is reflected in the shift in the CN stretching wavenumber from 2050–2090 cm^{-1} for Fe(II) to 2115–2125 cm^{-1} for Fe(III). This shift can be attributed to a shift in electron density through the pi-bonds of the cyano groups in going from hexacyanoferrate (III) to hexacyanoferrate (II). The Raman spectra of the hydrotalcite synthesized with hexacyanoferrate(II) and (III) in the interlayer are shown in Fig. 4. Three bands are observed at 2101, 2094 and 2059 cm^{-1} for the hexacyanoferrate(II) complex with an additional band at 2048 cm^{-1}, and four bands at 2127, 2118, 2099 and 2059 cm^{-1} for the hexacyanoferrate(III) interlayered hydrotalcite. Some earlier studies reported only
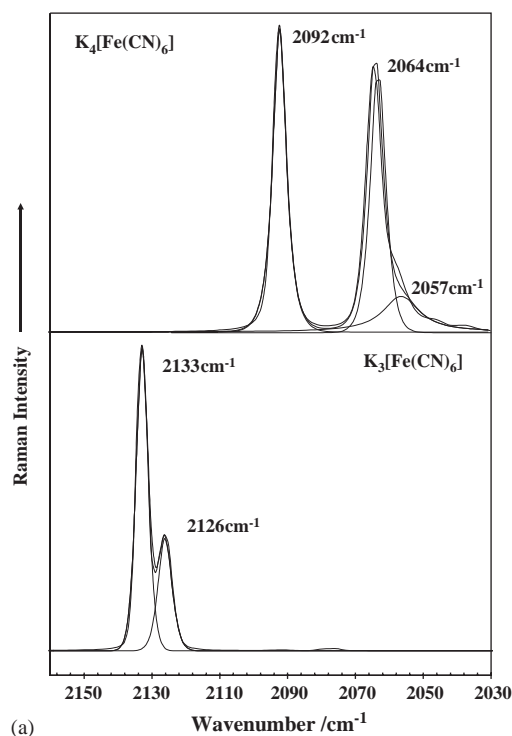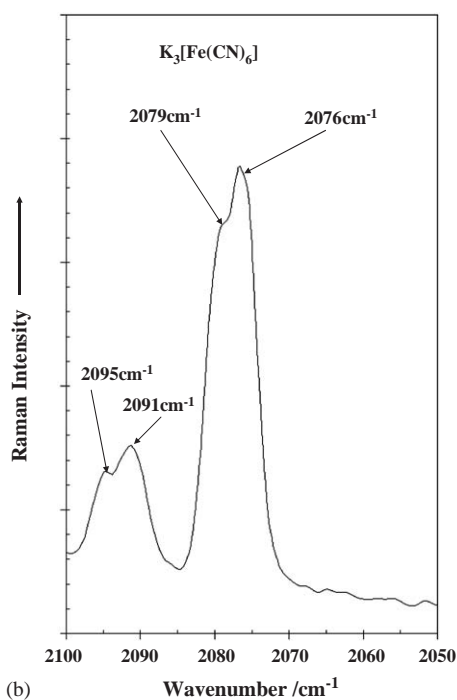
Fig. 2. (a) Raman spectra of the potassium salts of hexacyanoferrate(II) and (III). (b) Raman spectra of hexacyanoferrate (III) expanded in the 2050 to 2100 cm^{-1} region.
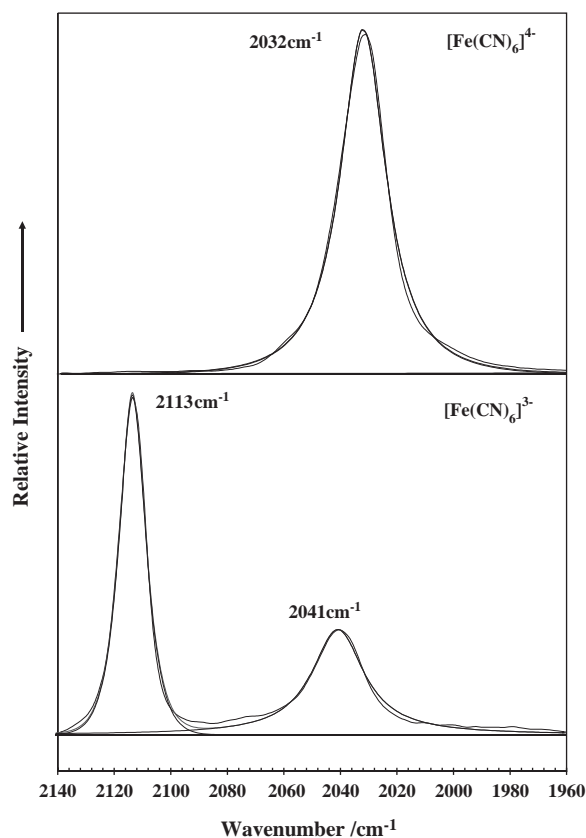

Fig. 3. Infrared spectra of the potassium salts of hexacyanoferrate(II) and (III).

[16]. Further Idemura et al. observed a reduction of the Fe in hexacyanoferrate(III) complexes by Mössbauer spectroscopy [45]. Crespo pointed out that the shift in position of the CN stretching wavenumber for the hexacyanoferrate(II) interlayered hydrotalcite was also influenced by the hydrogen bonding between the cyano groups and the interlayer water and also the hydroxyl surfaces of the brucite-like surface [12]. However, this concept is not supported by both the infrared and Raman data of the water and hydroxyl OH bending and stretching modes. In the infrared spectra the bending mode is at $1612 \, cm^{-1}$ and the OH stretching bands between 3000 and $3800 \, cm^{-1}$. Idemura et al. synthesized hydrotalcites with varying amounts of the hexacyano-ferrate(II) and (III) in the hydrotalcite through ion exchange from the nitrate interlayered hydrotalcite with the potassium and sodium hexacyano salt solutions with the exclusion of carbonate. Their infrared spectra showed two bands at 2120 and $2040 \, cm^{-1}$; thus indicating some partial reduction of the Fe(III) to (Fe(II) during intercalation. Their infrared work also showed that only a single band at $2040 \, cm^{-1}$ was observed when the sample was dried in vacuum and the second band appeared when the sample was dried in air. Similar observations have been reported by other groups [14–16,19].
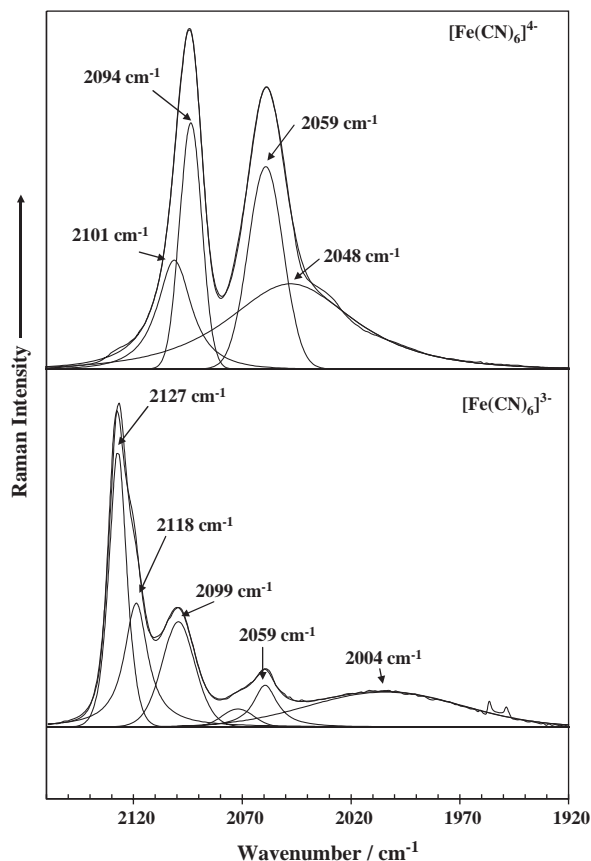
two bands for each of the hexacyanoferrate(II) and (III) interlayered hydrotalcites [12].

Holgadao et al. provided evidence based on Fe–K XANES measurements for the partial oxidation-reduction of the iron in the hexacyanoferrate hydrotalcite

Fig. 4. Raman spectra of the hexacyanoferrate(II) and (III) inter-layered Mg, Al hydrotalcite.

Fig. 5. Hot stage Raman spectra of the OH stretching region of the hexacyanoferrate(II) interlayered Mg, Al hydrotalcite.

3.3. Hot stage Raman spectroscopy

3.3.1. Thermal treatment of the hexacyanoferrate(II) interlayered hydrotalcite

The hot stage Raman spectra of the hexacyanoferra-te(II) in the OH stretching region and in the $2000–2150\,cm^{-1}$ region are shown in Fig. 5 and Fig. 6, respectively. The hot stage Raman spectra of the hexacyanoferrate(III) in the $2000–2150\,cm^{-1}$ region is shown in Fig. 7. The results of the Raman spectral analysis are reported in Tables 1 and 2. The Raman spectra of the Fe(II) hydrotalcite shows two bands at 2094 and $2059\,cm^{-1}$ with additional bands at 2048 and $2101\,cm^{-1}$. At $100\,^{\circ}C$ two bands are observed at 2098 and $2059\,cm^{-1}$ with two additional bands resolved at 2124 and $2071\,cm^{-1}$. In the $150\,^{\circ}C$ spectrum the intensity of the latter two bands increases. This intensity increases is observed in the $200\,^{\circ}C$ spectrum. In the $250\,^{\circ}C$ spectrum the two predominant bands are observed at 2119 and $2074\,cm^{-1}$. In the $300\,^{\circ}C$ spectrum a broad band is revealed at around $2084\,cm^{-1}$. This band corresponds to free CN^{-} ion and represents the HCN molecules which are being lost above $250\,^{\circ}C$. No intensity remains in the bands at around 2048 and $2094\,cm^{-1}$. It is proposed that the heating of the
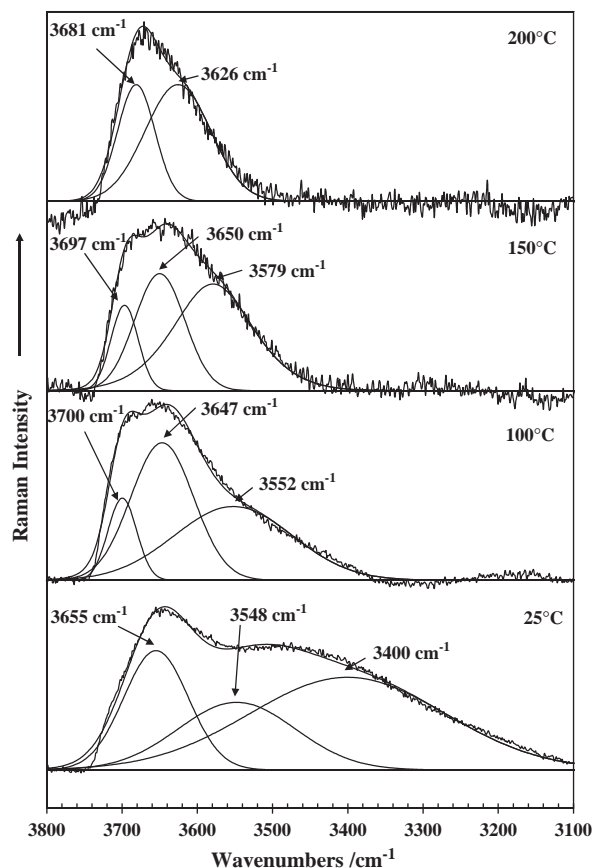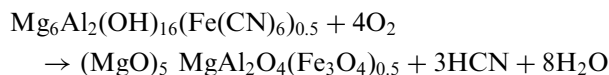
hexacyanoferrate(II) interlayered hydrotalcite intro-duces O_2 into the system and causes the oxidation of the Fe(II) to (Fe(III)). This oxidation is observed through the development of the additional peaks at around 2124 and $2070\,cm^{-1}$ which increase in intensity with thermal treatment.

Thermal analysis shows that HCN is lost at $270\,^{\circ}C$. The spectrum at $300\,^{\circ}C$ is too noisy to be curve resolved and at this temperature the structure of the hydrotalcite is lost. At $300\,^{\circ}C$ the hexacyanoferrate(II) hydrotalcite has decomposed according to the following reaction:

$$Mg_6Al_2(OH)_{16}(Fe(CN)_6)_{0.5} + 4O_2$$
$$\rightarrow (MgO)_5\ MgAl_2O_4(Fe_3O_4)_{0.5} + 3HCN + 8H_2O$$

XRD shows that the products of the thermal decomposition of the hexacyanoferrate(II) interlayered hydrotalcite are MgO, Mg_2AlO_4 (spinel) and Fe_3O_4.

The Raman spectra of the hydroxyl stretching region of the hexacyanoferrate(II) interlayered hydrotalcite are shown in Fig. 5. At $25\,^{\circ}C$ three bands are observed at 3655, 3548 and $3400\,cm^{-1}$. The first band is assigned to the hydroxyl stretching vibration of the brucite-like hydroxyl surface and the latter two bands are assigned
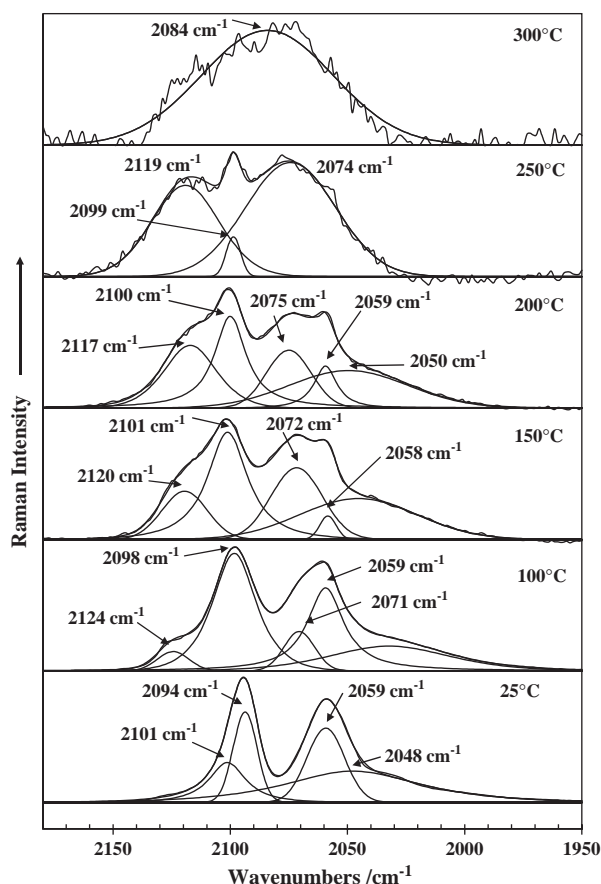
Fig. 6. Hot stage Raman spectra of the 1950 to 2150 cm^{-1} region of the hexacyanoferrate(II) interlayered Mg, Al hydrotalcite.

Fig. 7. Hot stage Raman spectra of the 1950 to 2150 cm^{-1} region of the hexacyanoferrate(III) interlayered Mg, Al hydrotalcite.

to water stretching bands. At 100 °C much of the intensity of the 3400 cm^{-1} band has diminished. Three bands are observed at 3700, 3647 and 3552 cm^{-1} in the 100 °C spectrum. Further heating results in the decrease in intensity of the band at 3552 cm^{-1}. Thermal analysis shows that dehydration of the hexacyanoferrate(II) interlayered hydrotalcite is complete by 150 °C. Thus the two bands in the 200 °C spectrum are attributed to the brucite-like hydroxyl stretching vibrations. Two bands are observed at 3681 and 3626 cm^{-1}. One possible assignment of these bands is to AlOH and MgOH stretching vibrations.

3.3.2. Thermal treatment of the hexacyanoferrate(III) interlayered hydrotalcite

The Raman spectra of the hexacyanoferrate(III) interlayered hydrotalcite (shown in Fig. 7) reveals four bands at 2127, 2119, 2099 and 2072 cm^{-1} at 25 °C. Significant changes are observed in the 100 °C spectrum. Four bands are observed at 2128, 2121, 2102 and 2072 cm^{-1}. In addition a broad feature is observed at 2080 cm^{-1}. This latter band is present in all the spectra and increases in intensity as the temperature is raised. The band is attributed to free CN^{-} ions. A previous
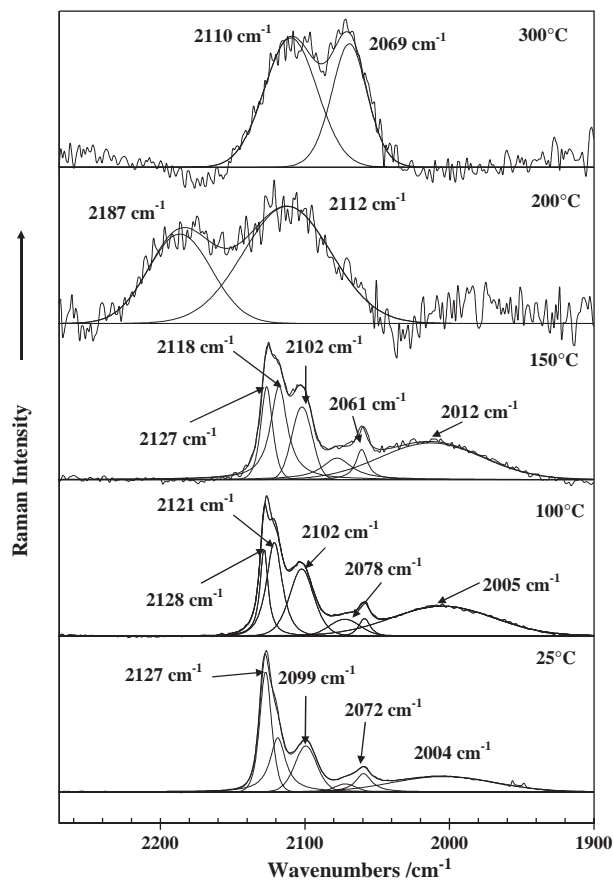
study considered the equilibrium between water or hydroxyls with the cyanide ion with water replacing the CN^{-} ion [25]. In this model the CN^{-} ions would not be expelled from the interlayer but rather retained in an equilibrium process. At the elevated temperatures with oxygen present it is more likely that the CN^{-} ions are expelled and the octahedral coordination of the Fe(III) maintained by bonding to oxygen. Hansen and Koch reported an infrared band at 2039 cm^{-1} and a sharp band at 2027 cm^{-1} [15]. They attributed these bands to free CN^{-} ions. However the band position for free CN^{-} ions is around 2080 cm^{-1}. This may simply mean that the CN^{-} ions have replaced the OH units on the brucite-like hydroxyl sheets. Such a reaction would release OH ions into the interlayer. The results of this and a previous study [25] do not support the concept of free CN^{-} ions in the interlayer as no bands are observed at 2027 or 2039 cm^{-1}. The observation of a broadish band at ~2080 cm^{-1} may mean that the CN^{-} ions have moved out of the interlayer and are adsorbed on the surface of the metal oxides which are being formed during the decomposition.

In the 150 °C spectrum four bands are observed at 2127, 2118, 2102 and 2061 cm^{-1}. The first two bands are

Table 1
Results of the Raman spectral analysis of the hexacyanoferrate(II) as a function of temperature

Room Temp.			100 °C			150 °C			200 °C			250 °C			300 °C		
Wave number	FWHM	%**	Wave number	FWHM	%	Wave number	FWHM	%	Wave number	FWHM	%	Wave number	FWHM	%	Wave number	FWHM	%
			3699.7	45.0	2.7	3696.7	42.6	2.4	3681.2	58.4	4.6						
3654.9	101.2	3.5	3646.7	98.1	4.9	3650.0	78.4	6.0									
									3625.7	102.5	4.1						
						3579.2	123.6	4.5									
3547.6	183.5	3.6	3552.2	184.7	4.9												
3400.5	306.6	16.3															
			2124.4	15.9	3.1	2119.5	22.7	6.7	2117.1	26.3	11.4	2119.2	33.9	11.5			
2101.3	18.4	10.2	2098.3	21.8	28.6	2101.2	20.3	16.4	2100.0	16.2	14.2	2098.7	7.3	1.1			
2093.7	12.0	12.4													2084.3	66.4	27.3
			2070.6	15.5	6.1	2071.7	25.8	11.3	2075.1	22.5	8.5	2074.3	45.3	18.9			
2059.3	18.9	16.0	2059.4	18.7	22.8	2058.4	8.3	1.2	2059.4	11.6	4.0						
2047.8	67.3	26.8	2032.2	60.4	15.7	2045.5	59.0	14.7	2049.6	59.7	14.7						
						1548.1	76.8	6.9	1555.8	95.5	15.7	1541.1	92.2	48.0	1544.9	84.7	52.9
						1493.6	51.4	12.5	1498.7	53.3	8.3						
												1276.4	36.1	2.3			
						1113.4	44.8	11.6	1117.6	49.5	10.9	1122.7	47.7	15.5	1121.1	63.3	19.8
						1016.3	39.7	1.0									
698.7	34.6	0.5															
586.8	31.4	0.9															
507.5	21.2	1.0	507.0	17.7	0.5	510.3	17.2	0.3									
476.7	32.9	1.4	472.5	34.5	1.5	471.8	13.4	0.2									
			361.7	46.2	0.5												
288.6	42.3	1.2	277.1	82.6	2.5												
						257.4	56.8	1.4	241.8	25.1	0.8						
233.0	57.0	1.9	218.8	45.1	2.3	223.7	41.3	1.7	224.0	12.6	0.7	224.1	12.1	1.3			
196.3	41.3	1.9	195.2	26.8	1.1				192.7	18.5	0.9	202.8	9.7	1.3			

** % Relative intensity.

Table 2
Results of the Raman spectral analysis of the hexacyanoferrate(III) as a function of temperature

Room Temp			100 °C			150 °C			200 °C			300 °C		
Wave number	FWHM	%**	Wave number	FWHM	%	Wave number	FWHM	%	Wave number	FWHM	%	Wave number	FWHM	%
3715.7	23.0	0.8												
3688.0	46.9	1.4	3696.5	42.6	1.8	3692.3	31.0	0.9						
3633.1	100.9	3.3	3622.1	107.4	9.7	3633.7	90.1	3.1						
3531.5	200.2	4.2												
									2186.5	51.6	5.5			
2127.2	9.5	15.4	2128.3	6.6	6.4	2126.5	9.5	5.1						
2118.8	12.9	12.8	2121.2	12.7	11.3	2118.0	13.9	10.1						
2099.4	17.9	10.6	2102.3	19.8	11.4	2102.0	16.5	6.3	2112.3	71.5	10.0	2109.8	42.9	19.2
2072.1	17.3	1.7	2072.5	24.7	3.4	2077.9	24.6	4.1				2069.3	29.0	12.7
2059.5	13.2	4.0	2058.8	9.1	1.4	2060.7	9.6	2.3						
2004.3	83.5	15.9	2004.7	82.9	20.3	2012.6	83.8	16.2						
						1544.9	75.1	18.4				1545.1	84.5	32.3
			1516.1	103.2	7.9				1527.4	97.6	54.4			
						1496.8	57.5	13.4						
			1113.5	49.5	3.0	1121.8	49.1	17.0	1124.5	55.8	30.0	1116.5	67.4	16.3
												1058.7	67.7	19.5
810.6	104.6	3.3												
			780.5	127.8	7.4									
732.6	80.0	5.3												
686.0	50.0	2.5	700.3	57.9	3.8									
587.9	22.9	1.0	588.5	17.9	0.5									
505.1	37.6	1.6	505.6	41.5	1.5									
468.7	26.1	1.2	466.8	22.3	0.8									
369.9	58.6	2.9	369.0	41.6	1.4									
301.2	53.9	3.5	309.6	43.5	1.6									
247.3	62.6	4.0	252.9	71.2	4.0	258.9	41.6	1.7						
205.4	31.1	0.9	206.8	10.7	0.3	204.7	13.9	1.3						

** % Relative intensity.

assigned to the CN stretching vibrations of the hexacyanoferrate(III) interlayered hydrotalcite and the second two bands are assigned to the CN stretching vibrations of the hexacyanoferrate(II) interlayered hydrotalcite. The potassium hexacyanoferrate(III) salt used in the experiment showed only very low concentrations of the hexacyanoferrate(II) ion. Thus it is concluded that during the synthesis of the hexacyanoferrate(III) interlayered hydrotalcite some reduction of Fe(III) to Fe(II) occurred. At temperatures above 150 °C, the spectral features of the hexacyanoferrate(III) interlayered hydrotalcite are lost. At 200 °C two broad bands are observed at 2187 and 2112 cm^{-1}. The spectra suffer from a lack of signal-to-noise, as the thermal background in the spectra increases greatly at the higher temperatures.

Thermal decomposition as determined by thermogravimetric methods shows that the hexacyanoferrate(III) interlayered hydrotalcite is dehydrated by 150 °C. This accounts for the very significant changes in the spectra in going from 150 to 200 °C. TGA coupled to a gas evolution mass spectra also shows that the cyanide ion is lost above 200 °C. Dehydration as determined by gas evolution mass spectrometry shows that dehydra-

tion has occurred by 150 °C. The loss of the CN ions occurs simultaneously as the dehydroxylation of the hexacyanoferrate(III) interlayered hydrotalcite occurs. The cyanide ion is lost as cyanic acid. This shows that the cyanide ion reacts with the hydroxyl surface of the hexacyanoferrate(III) interlayered hydrotalcite to produce HCN with the oxygen bonded to the cations of the hydrotalcite Such a concept has been previously suggested [15].

4. Conclusions

Raman spectroscopy confirms the intercalation of hexacyanoferrate(II) and (III) in the interlayer of Mg, Al hydrotalcite with the partial reduction of the hexacyanoferrate(III) interlayered hydrotalcite and the partial oxidation of the hexacyanoferrate(II) interlayered hydrotalcite. This results in a mixed valence combination in the interlayer irrespective of the initial starting hexacyanoferrate. Hot stage Raman spectroscopy shows that the hexacyanoferrate(II) interlayered hydrotalcite undergoes oxidation to the hexacyanoferrate(III) interlayered hydrotalcite before decomposition

at 250 °C. The hexacyanoferrate(III) interlayered hydro-talcite remains stable up to 150 °C after which decomposition with the loss of cyanide ions occurs. Free cyanide is lost during the thermal treatment of the hexacyanoferrate(III) hydrotalcite.

Acknowledgments

References

[1] V. Rives and Editor, Layered Double Hydroxides: Present and Future, 2001.

[2] R.L. Frost, W.N. Martens, L. Duong, J.T. Kloprogge, J. Mater. Sci. Lett. 21 (2002) 1237.

[3] R.L. Frost, Z. Ding, W.N. Martens, T.E. Johnson, J.T. Kloprogge, Spectrochim. Acta A 59A (2003) 321.

[4] R.L. Frost, W. Martens, Z. Ding, J.T. Kloprogge, T.E. Johnson, Spectrochim. Acta A 59A (2003) 291.

[5] L. Hickey, J.T. Kloprogge, R.L. Frost, J. Mater. Sci. 35 (2000) 4347.

[6] T.E. Johnson, W. Martens, R.L. Frost, Z. Ding, J.T. Kloprogge, J. Raman Spectrosc. 33 (2002) 604.

[7] J.T. Kloprogge, L. Hickey, R.L. Frost, Appl. Clay Sci. 18 (2001) 37.

[8] J.T. Kloprogge, D. Wharton, L. Hickey, R.L. Frost, Am. Mineral. 87 (2002) 623.

[9] R.M. Taylor, Clay Minerals 17 (1982) 369.

[10] H.F.W. Taylor, Mineral. Mag. J. Mineral. Soc. (1876–1968) 37 (1969) 338.

[11] A.H. Iglesias, O.P. Ferreira, D.X. Gouveia, A.G. Souza Filho, J.A.C. De Paiva, J. Mendes Filho, O.L. Alves, J. Solid State Chem. 178 (2005) 142.

[12] I. Crespo, C. Barriga, V. Rives, M.A. Ulibarri, Solid State Ionics 101–103 (1997) 729.

[13] I. Carpani, M. Berrettoni, B. Ballarin, M. Giorgetti, E. Scavetta, D. Tonelli, Solid State Ionics 168 (2004) 167.

[14] J.M. Fernandez, M.A. Ulibarri, F.M. Labajos, V. Rives, J. Mater. Chem. 8 (1998) 2507.

[15] H.C.B. Hansen, C.B. Koch, Clays Clay Minerals 42 (1994) 170.

[16] M.J. Holgado, V. Rives, M.S. Sanroman, P. Malet, Solid State Ionics 92 (1996) 273.

[17] K. Itaya, H.C. Chang, I. Uchida, Inorganic Chem. 26 (1987) 624.

[18] S. Kikkawa, M. Koizumi, Mater. Res. Bull. 17 (1982) 191.

[19] K. Yao, M. Taniguchi, M. Nakata, A. Yamagishi, J. Electroanal. Chem. 458 (1998) 249.

[20] J. Labuda, M. Hudakova, Electroanalysis 9 (1997) 239.

[21] B.R. Shaw, Y. Deng, F.E. Strillacci, K.A. Carrado, M.G. Fessehaie, J. Electrochem. Soc. 137 (1990) 3136.

[22] K. Okada, F. Matsushita, S. Hayashi, A. Yasumori, Clay Sci. 10 (1996) 1.

[23] K. Yao, M. Taniguchi, M. Nakata, M. Takahashi, A. Yamagishi, Langmuir 14 (1998) 2890.

[24] H.C.B. Hansen, C.B. Koch, Appl. Clay Sci. 10 (1995) 5.

[25] J.T. Kloprogge, M. Weier, I. Crespo, M.A. Ulibarri, C. Barriga, V. Rives, W.N. Martens, R.L. Frost, J. Solid State Chem. 177 (2004) 1382.

[26] L. Frost Ray, L. Weier Matt, E. Clissold Meagan, A. Williams Peter, Spectrochim. Acta A 59 (2003) 3313.

[27] R.L. Frost, M.L. Weier, M.E. Clissold, P.A. Williams, Spectrochim. Acta A 59A (2003) 3313.

[28] R.L. Frost, M.L. Weier, J.T. Kloprogge, J. Raman Spectrosc. 34 (2003) 760.

[29] D.L. Bish, A. Livingstone, Mineral. Mag. 44 (1981) 339.

[30] E.H. Nickel, R.M. Clarke, Am. Mineral. 61 (1976) 366.

[31] O.P. Ferreira, O.L. Alves, D.X. Gouveia, A.G. Souza Filho, J.A.C. De Paiva, J.M. Filho, J. Solid State Chem. 177 (2004) 3058.

[32] F. Rey, V. Fornes, J.M. Rojo, J. Chem. Soc., Faraday Trans. 88 (1992) 2233.

[33] M. Valcheva-Traykova, N. Davidova, A. Weiss, J. Mater. Sci. 28 (1993) 2157.

[34] G. Lichti, J. Mulcahy, Chem. Australia 65 (1998) 10.

[35] Y. Seida, Y. Nakano, J. Chem. Eng. Japan 34 (2001) 906.

[36] Y. Roh, S.Y. Lee, M.P. Elless, J.E. Foss, Clays Clay Minerals 48 (2000) 266.

[37] Y. Seida, Y. Nakano, Y. Nakamura, Water Res. 35 (2001) 2341.

[38] R.L. Frost, K.L. Erickson, J. Thermal Anal. Calorimetry 76 (2004) 217.

[39] E. Horvath, J. Kristof, R.L. Frost, N. Heider, V. Vagvoelgyi, J. Thermal Anal. Calorimetry 78 (2004) 687.

[40] R.L. Frost, M.L. Weier, K.L. Erickson, J. Thermal Analy. Calorimetry 76 (2004) 1025.

[41] R.L. Frost, K.L. Erickson, J. Thermal Anal. Calorimetry 78 (2004) 367.

[42] E. Horvath, J. Kristof, R.L. Frost, A. Redey, V. Vagvolgyi, T. Cseh, J. Thermal Anal. Calorimetry 71 (2003) 707.

[43] J. Kristof, R.L. Frost, J.T. Kloprogge, E. Horvath, E. Mako, J. Thermal Anal. Calorimetry 69 (2002) 77.

[44] P.S. Braterman, C. Tan, J. Zhao, Mater. Res. Bull. 29 (1994) 1217.

[45] S. Idemura, E. Suzuki, Y. Ono, Clays Clay Minerals 37 (1989) 553.